Spectroscopic investigation of $CaAl_{12}O_{19}:M^{3+}$ upon UV/vacuum–UV excitation: a comparison with $SrAl_{12}O_{19}:M^{3+}$ (M = Pr,Cr)

Spectroscopic investigation of $CaAl_{12}O_{19}:M^{3+}$ upon UV/vacuum–UV excitation: a comparison with $SrAl_{12}O_{19}:M^{3+}$ (M = Pr, Cr)

Zhaogang Nie[1,2]**, Jiahua Zhang**[1,2,5]**, Xia Zhang**[1,2]**, Xinguang Ren**[1,2]**, Weihua Di**[1,2]**, Guobin Zhang**[3]**, Danhong Zhang**[3] **and X-J Wang**[1,2,4,5]

[1] Key Laboratory of Excited State Physics, Changchun Institute of Optics, Fine Mechanics and Physics, Chinese Academy of Sciences (CAS), Changchun 130033, People's Republic of China
[2] Graduate School of CAS, Beijing 100039, People's Republic of China
[3] National Synchrotron Radiation Laboratory, University of Science and Technology of China, Hefei 230029, People's Republic of China
[4] Department of Physics, Georgia Southern University, Statesboro, GA 30460, USA

E-mail: zjiahua@public.cc.jl.cn and xwang@georgiasouthern.edu

Abstract

In order to evaluate the possibility of using Cr^{3+} co-doping to modify the emission properties of Pr^{3+}-based quantum cutting phosphors, which emit one ultraviolet (UV) and one visible photon from each vacuum–UV photon absorbed, into phosphors that emit two visible photons, the optical spectroscopies between 150 and 750 nm of $CaAl_{12}O_{19}:M^{3+}$ (M = Pr, Cr) were investigated and compared with those of $SrAl_{12}O_{19}:M^{3+}$ using synchrotron radiation as one of the excitation sources. When Pr^{3+} is excited to its 4f5d states, cascade emission of UV photons from the $^1S_0$ state followed by visible photons from the $^3P_0$ state are both observed in $(Ca, Sr)Al_{12}O_{19}:Pr^{3+}$. Similar to $SrAl_{12}O_{19}:M^{3+}$, there exist desirable spectral overlaps between Pr^{3+} $^1S_0$ emissions and the Cr^{3+} higher multiplet absorptions in $CaAl_{12}O_{19}$, which should be favourable to the energy transfer from Pr^{3+} $^1S_0$ to Cr^{3+}, converting the UV photon from Pr^{3+} $^1S_0$ into the red Cr^{3+} emission. However, the host absorption band and the Cr^{3+}-related charge transfer band have an unfavourable overlap with the Pr^{3+} 4f5d states in the vacuum–UV region, preventing efficient selective Pr^{3+} excitation under radiation of Xe discharge, a prerequisite for the quantum cutting process.

1. Introduction

Recently, a growing interest has arisen in investigations on highly efficient vacuum–UV (VUV) excited phosphors triggered by the applications of mercury-free fluorescent tubes and plasma

---

[5] Authors to whom any correspondence should be addressed.
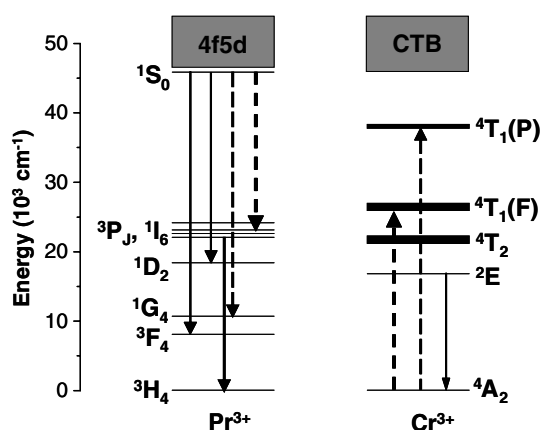
Figure 1. Part of the energy level diagram of the Pr^{3+}–Cr^{3+} pair in the CAO (or SAO) system. The dashed lines indicate possible nonradiative energy transfer processes from Pr^{3+} to Cr^{3+}. For the sake of clarity, the energy level schemes of the ions are simplified.

displays [1]. In these devices, the phosphors used nowadays convert one VUV photon from the noble gas discharge into one visible photon by dissipating roughly half of the absorbed energy into heat. However, the high energy of the VUV photon makes it theoretically possible to achieve two visible photon emissions for one VUV photon absorbed to obtain 200% quantum efficiency (QE). This phenomenon is called visible quantum cutting (QC) or photon cascade emission [2].

The discovery of QC systems started with the findings of Pr^{3+} ions capable of cascade emissions in fluorides [3, 4]. In general, when Pr^{3+} is excited to its 4f5d states, visible QC through a cascade emission due to $^1S_0 \rightarrow {}^1I_6$ around 402 nm followed by $^3P_0 \rightarrow {}^3H_4$ radiation around 485 nm could occur in some Pr^{3+} doped hosts in which the $^1S_0$ (4f^2) level is located below the lowest 4f5d state (see figure 1). Thus, a system with internal quantum efficiency (QE) greater than unity can be achieved. By now, more than a dozen of such Pr^{3+}-based QC phosphors, including some oxide materials [5–8], have been identified, but they have been found unsuitable for practical applications because the first step transition of Pr^{3+} is in the UV region, which is unsuitable for practical applications. An appropriate co-dopant which can convert this first step photon to a proper visible photon through energy transfer (ET) could be a solution for this situation. The ET efficiency of the Forster–Dexter type depends on the spectral overlap between Pr^{3+} emission and co-activator absorption as well as on their separation [9, 10]. Both strongly depend on the type of host lattice. In recent years, research work has been done in many systems in order to find good hosts, in which Pr^{3+} shows the QC phenomena, and good co-activators to improve the colour rendering of Pr^{3+} emissions [11–16].

In this work, the hosts $CaAl_{12}O_{19}$ (CAO) and $SrAl_{12}O_{19}$ (SAO) were selected to incorporate Pr^{3+} and Cr^{3+}. CAO and SAO are isomorphic crystals. They are convenient oxide materials for rare-earth (RE) and transition-metal dopants and are also suitable host crystals for Pr^{3+} QC [5, 17]. Wang *et al* have reported the observation of ET between Pr^{3+} and Er^{3+} in CAO [14]. However, both RE ions replacing Ca ions enter the host. The large donor–acceptor (D–A) distance results in a small D–A interaction, giving a small ET rate. The Cr^{3+} ion was chosen as a suitable co-activator ion because (i) it has efficient red emissions in the two hosts and has abundant absorption transitions to match the Pr^{3+} $^1S_0$ emissions (see figure 1) and (ii) it is expected that Cr^{3+} replaces Al^{3+} in the host. The average Ca–Al distance is shorter than the Ca–Ca distance [18, 19], benefiting efficient ET from Pr^{3+} to Cr^{3+}.

ET between Pr^{3+} and Cr^{3+} in SAO has been observed by us [20, 21]. The transfer can convert the $^1S_0$ UV fluorescence of Pr^{3+} into the red emission of Cr^{3+}. However, a practical QC phosphor based on the Pr^{3+}–Cr^{3+} pair can only be successful when (i) the Pr^{3+} ion in the host has higher VUV absorption efficiency for the emission of a Xe gas discharge, (ii) the $Pr^{3+} \rightarrow Cr^{3+}$ transfer is efficient, and (iii) the spectra properties of Cr^{3+} are fit for the practical applications. In this paper, the excitation and emission properties of Cr^{3+} focusing on the Cr^{3+} crystal-field sites, the spectra properties of the higher-energy excited states of Pr^{3+}, the effects of host excitation in the VUV region on Pr^{3+} luminescence, and finally the spectra overlaps between the two ions in CAO, will therefore be systematically investigated and compared with those in SAO.

2. Experiment procedures

2.1. Sample preparation

Microcrystalline CAO:M^{3+} (M = Pr, Cr) and SAO:M^{3+} phosphors were synthesized by solid-state reactions under a CO reduction atmosphere with the corresponding oxides (high-purity reagents) as the starting materials. The Pr^{3+} and Cr^{3+} ions replace Ca^{2+} (or Sr^{2+}) and Al^{3+}, respectively, in the host. When Pr^{3+} is doped, an equal amount of Mg^{2+} was added to substitute Al^{3+} for charge compensation.

2.2. Measurements

All the measurements were performed at room temperature. The microcrystalline samples were verified to be in single phase by x-ray diffraction. The VUV spectra were measured at the VUV station of the BS-U10B beam-line in the National Synchrotron Radiation Laboratory (Heifei, China) and the excitation spectra in the range 140–350 nm were corrected using the excitation spectrum of sodium salicylate as a standard. Fluorescence and excitation spectra in the UV region were obtained on a Hitachi F-4500 fluorescence spectrophotometer. The spectra were corrected for the photon flux of the excitation light. The high-resolution emission spectra were recorded by a Spex 1403 spectrometer, a photomultiplier, and a boxcar integrator, and were processed by a computer. For lifetime measurements, the signal was detected with a Tektronix digital oscilloscope (model TDS 3052). An optical parametric oscillator was used as the excitation source. It has a line width of 0.2 cm^{-1}, pulse duration of 10 ns, and repetition frequency of 10 Hz.

3. Results and discussion

3.1. Excitation and emission properties of Cr^{3+}

Figure 2 shows the excitation and emission spectra of CAO:Cr^{3+} (a) and SAO:Cr^{3+} (b), respectively. The principal features of the UV excitation spectra for both spectra are three broad bands which belong to the spin-allowed electronic transitions from the $^4A_2$ to the $^4T_2$, $^4T_1$ (^4F) and $^4T_1$ (^4P) states. Two weaker sharp lines due to the spin-forbidden transitions of $^4A_2$ to $^2T_1$, $^2T_2$ levels are observed. The UV excitation bands of CAO:Cr^{3+} shift slightly to higher energies in comparison with those of SAO:Cr^{3+}. However, no obvious shifts of the lines of $^2T_{1,2}$ levels can be found. Similar observations have been made for Cr^{3+} ions in other compounds [22, 23]. In the VUV region, the broad bands dominating the absorptions at about 184 nm for CAO:1% Cr^{3+} and 180 nm for SAO:1% Cr^{3+}, respectively, are ascribed to the O^{2-}–Cr^{3+}-related charge transfer bands (CTBs) [24]. In contrast to the UV excitation bands, the CTB in CAO:Cr^{3+} shifts slightly to lower energy than that in SAO:Cr^{3+}. The emission
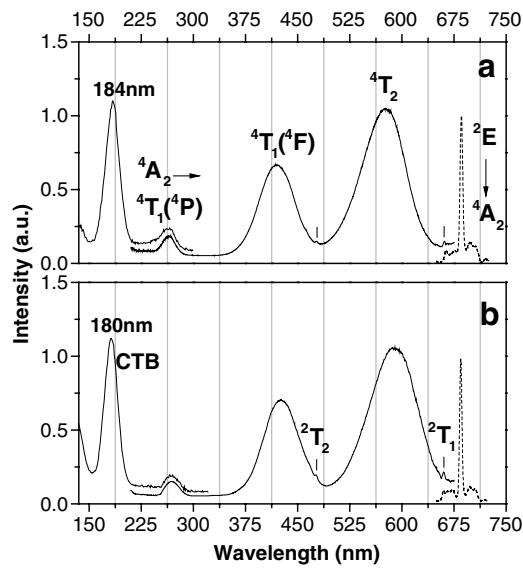
**Figure 2.** Excitation (solid) and emission (dashed) spectra of CAO:1% Cr^{3+} (a) and SAO:1% Cr^{3+} (b), monitoring the Cr^{3+} emission at 686 and 685 nm, respectively. The UV and VUV excitation spectra are scaled to the $^4A_2 \rightarrow {}^4T_1(^4P)$ excitation intensity.

spectra are the typical emissions of Cr^{3+}, which both consist of a narrow $^2E \rightarrow {}^4A_2$ zero-phonon line (R-line) peaking at 686 and 685 nm for CAO and SAO, respectively, with vibronic sidebands [23]. The emission feature is independent of the excitation band reached, even for the CTB in VUV region, and no other emissions can be observed.

CAO is isomorphic to SAO. The unit cell of CAO (or SAO) is shown in figure 3. It adopts a hexagonal magnetoplumbite structure with a 12-fold coordinated Ca^{2+} site and five different Al^{3+} sites, among them three with AlO_6 octahedra [18, 19]. Due to charge neutrality and the ion size of Cr^{3+}, the trivalent Cr ions (75.5 pm, 6-coord.; all radii taken from [26]) will prefer to replace trivalent Al ions (67.5 pm, 6-coord.) instead of the divalent and considerably larger Ca ions ($\sim$126 pm). In addition, Cr^{3+} ions ($3d^3$) tend to occupy approximately octahedral sites [25]. In a wide variety of metal oxide host systems, Cr^{3+} ions are invariably oxygen-coordinated with six nearest neighbours, possibly in a pure octahedral or a distorted octahedral symmetry site. According to ligand-field theory, the features of the excitation and emission spectra, i.e., the spectral properties of the energy states of Cr^{3+} in CAO and SAO, indicate that the Cr^{3+} enters distorted octahedral sites [23]. Only Al ions occupy octahedral sites in this system. Thus, the Cr^{3+} ions replacing Al^{3+} ions enter the host.

As shown in figure 3, the neighbouring Ca sites, lying in the mirror plane containing Al ions, are separated by a rather formidable obstacle, i.e., a spinel-like block also containing Al ions. The Ca–Ca distance in the unit cell is about 10.95 Å. It is much larger than the average separation of Ca–Al ($\sim$4.64 Å) [18]. Thus, for the ET form Pr^{3+} to Cr^{3+}, the average D–A distance for Cr^{3+} co-doping is shorter than that for RE^{3+} co-doping for the same doping concentration. The shorter D–A distance may promote the ET between Pr^{3+} and Cr^{3+}.

Although there are different octahedral sites of Al^{3+} ions in the host lattice, only one site of Cr^{3+} emission is observed. Considering the same crystal structures of CAO and SAO and the similarities of the optical properties between Cr^{3+} in the two hosts, we believe that the Cr^{3+} ions should be at the same octahedral site in the two hosts. We name the two Cr^{3+} sites in CAO and SAO as sites Ω_C and Ω_S, respectively.
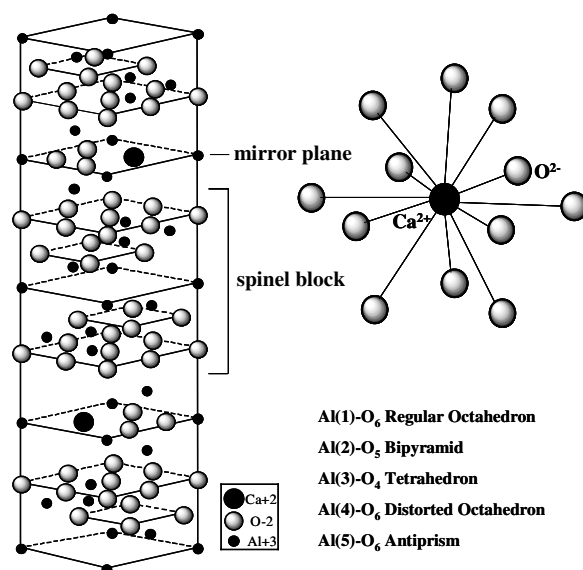
Figure 3. Unit cell of CAO (or SAO, space group P6$_3$/*mmc*) and Ca (or Sr) coordination polyhedron. The coordinations of various Al sites are given.

As the 3d electrons occupy the orbits on the outside of the ions, the optical spectroscopic properties of Cr^{3+} are sensitive to the environment. In ligand-field theory, the environmental effects are expressed by the magnitudes of Dq, the crystal-field parameter, and B and C, the Racah parameters [23]. The energies of the $^4T_2$, $^4T_1(^4F)$ and $^4T_1(^4P)$ states are highly sensitive to the crystal-field environment of the ion and vary linearly with Dq. Vibrational modulation of the field strength to these states produces the broad bands. However, as regards the ^2E and $^2T_{1,2}$ levels, their energies are insensitive to vibrational modulation and they therefore appear as sharp lines. From the positions of the excitation bands and the zero-phonon transitions, the spectroscopic parameters, Dq, B and C for sites Ω_C and Ω_S can be determined [27]. And then, the energy for the most relevant states of Cr^{3+}, taking the energy of the $^4A_2$ state equal to zero, can be calculated using the parameters found above [22]. For this purpose, the Tanabe–Sugano energy matrices are used for a d^3 configuration [27]. Dq and B are fixed by the $^4T_2$ and $^4T_1(^4F)$ band positions, respectively, and C is varied to provide the best fit to the ^2E transition. The crystal-field and Racah parameters obtained for the Cr^{3+} in site Ω_C are $Dq = 1736$ cm^{-1}, $B = 632$ cm^{-1} and $C = 3241$ cm^{-1}. The same parameters calculated for site Ω_S are, respectively, 1697, 648 and 3230 cm^{-1}. The Dq of the site Ω_C is larger than that of site Ω_S, which is consistent with the slight blue shift of excitation bands of site Ω_C. In addition, the blue shift is also in accord with the fact that the relevant ligand (O)–metal (Al) distance for the similar coordination surroundings in CAO is slightly less than that in SAO [19], which increases the crystal-field strength and, consequently, shifts the bands to higher energies. In the VUV spectra, the CT, which promotes an electron from the neighbouring $O^{2-}(2p^6)$ orbital to the empty levels of the central cation, also depends strongly on the ligand–metal distance [28]. However, the shorter Al–O distance in CAO means that the transfer of one electron from O^{2-} to Cr^{3+} needs less energy than that in SAO. As a result, the energy of the CTB in CAO decreases. As regards the sharp lines of $^2T_{1,2}$ levels, their energies are insensitive to Dq and therefore no obvious energy shifts can be observed. In addition, it can be verified that the value for the Dq/B ratio of the site Ω_C is 2.75, which is larger than that of the intermediate crystal field
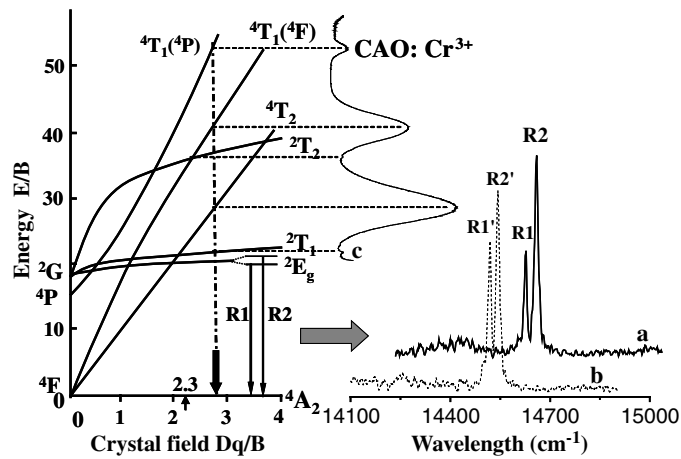
Figure 4. Tanabe–Sugano diagram for the main spectroscopic states of Cr^{3+} ($3d^3$) in an octahedral crystal field and the high-resolution emission spectra of CAO:Cr^{3+} (a) and SAO:Cr^{3+} (b). The corresponding excitation spectrum of CAO:Cr^{3+} as a reference is also shown (c).

($Dq/B \approx 2.3$) [23] and also larger than that of site Ω_S ($Dq/B = 2.62$). The Dq/B values in both sites are typical of strong crystalline fields.

Figure 4 presents the Tanabe–Sugano diagram for the main spectroscopic states of Cr^{3+} in an octahedral crystal field and the high-resolution emission spectra of CAO:Cr^{3+} (a) and SAO:Cr^{3+} (b). The corresponding excitation spectrum of CAO:Cr^{3+} as a reference is shown as well. The narrow Cr^{3+} R-line emission can be distinguished clearly. For site Ω_C, two sharp lines (R_1 and R_2) are located at 14 490.7 and 14 524.3 cm^{-1} and for Ω_S (R_1' and R_2'), 14 520.1 and 14 543.3 cm^{-1}, respectively. The spin–orbit coupling and the lowering of site symmetry act together, leading to ^2E level splitting [23]. From the positions of the R-lines the splittings can be evaluated; they are about 33.6 and 23.2 cm^{-1} for Ω_C and Ω_S, respectively, which are close to the values obtained in the literature for other oxide compounds [29]. The vertical broken line represents the appropriate value for Dq/B (2.75) evaluated for Ω_C. Luminescence of any octahedral coordinate Cr^{3+} system is determined by the relative energies and the sequence of the two lowest excited states, ^2E and $^4T_2$. From the diagram it is clear that the ^2E state corresponds to the lowest energy level, which is consistent with the sharp R-line emissions of Cr^{3+} due to the $^2E \rightarrow {}^4A_2$ transition in CAO. For site Ω_S, the Dq/B ratio is also larger than 2.3, and it also should represent the R-line emissions.

Figure 5 displays the fluorescence decay curves of the Cr^{3+} $^2E \rightarrow {}^4A_2$ transitions in CAO:1% Cr^{3+} (a) and SAO:1% Cr^{3+} (b), respectively. The Cr^{3+} $^2E \rightarrow {}^4A_2$ emissions from both systems decay exponentially. The lifetimes were determined to be 4.31 ms in CAO and 3.01 ms in SAO. The decay times in the ms range are typical compared to Cr^{3+} ^2E emissions in a high-crystal-field site [30]. The energy separation (Δ) between ^2E and $^4T_2$ levels contributes to the different decay times for both Cr^{3+} emissions [18]. The $^2E \rightarrow {}^4A_2$ transition is spin forbidden and becomes partially spin allowed due to spin–orbit coupling (ζ) of the ^2E and $^4T_2$ states. Stronger ζ leads to a higher degree of mixing the ^2E and $^4T_2$ levels and to a decreased lifetime of ^2E. The $^4T_2$ states situate at higher energy in CAO than that in SAO (see figure 2). The larger Δ in CAO results in a reduced admixture of ^2E into $^4T_2$, a decreased ζ of the ^2E and $^4T_2$ levels, and a lengthening of the lifetime.

6
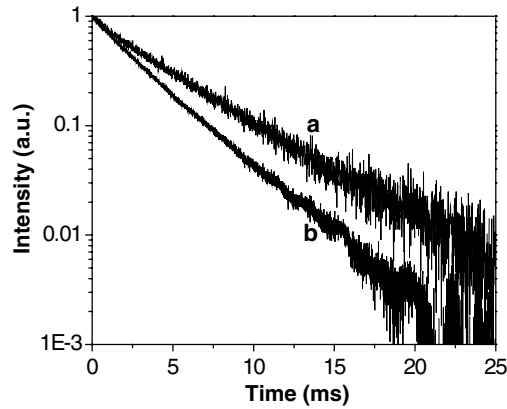
Figure 5. Fluorescence decay curves of the $^2E \rightarrow {}^4A_2$ transition in CAO:1% Cr^{3+} (a) and SAO:1% Cr^{3+} (b).
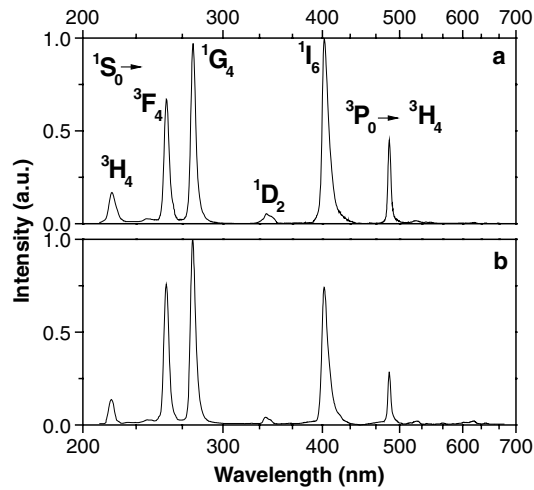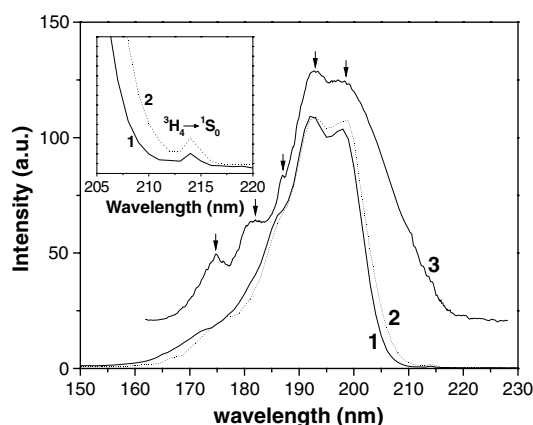

Figure 6. Emission spectra of CAO:1% Pr^{3+} (a) and SAO:1% Pr^{3+} (b) upon 4f5d excitation at 198 nm.

3.2. Excitation and emission properties of Pr^{3+}

Figure 6 presents the normalized and corrected emission spectra of CAO:Pr^{3+} (a) and SAO:Pr^{3+} (b) upon 4f5d excitation at 198 nm. The emission lines at 215, 254, 275, 341, and 402 nm are assigned to $^1S_0 \rightarrow {}^3H_4$, $^3F_4$, $^1G_4$, $^1D_2$, and $^1I_6$ transitions, respectively. The line at 485 nm is ascribed to the transition $^3P_0 \rightarrow {}^3H_4$. The emissions of the $^1S_0 \rightarrow {}^1I_6$ and $^3P_0 \rightarrow {}^3H_4$ transitions constitute the QC process in this system [5]. Neglecting the infrared transitions, the intensity ratio between the integrated $^3P_0$ emissions and the $^1S_0 \rightarrow {}^1I_6$ emission is equal to the QE of $^3P_0$, which is the intermediate state in the QC process. In this work, for CAO:1% Pr^{3+} the QE of $^3P_0$ is found to be about 78%, which is higher than that of SAO:1% Pr^{3+} (∼63%). Similar results have been reported in [31].

Figure 7 shows the VUV excitation spectra of SAO:1% Pr^{3+} (curve 1) and CAO:1% Pr^{3+} (curve 2) monitoring the $^1S_0 \rightarrow {}^1I_6$ emission at 402 nm. The common bands centred at about

Figure 7. VUV excitation spectra of SAO:1% Pr^{3+} (curve 1) and CAO:1% Pr^{3+} (curve 2), monitoring the $^1S_0 \rightarrow {}^1I_6$ emission at 402 nm. The excitation spectrum of CAO:2%Ce^{3+} (curve 3) is shown as well, by shifting the energy scale of the Ce^{3+} spectrum by 12 240 cm^{-1} relative to the Pr scale.

170 nm are due to the band-to-band excitation of the hosts [8]. The other bands are due to the excitations of Pr^{3+} $4f^2 \rightarrow 4f5d$ transitions [5]. For the rare-earth ions in a crystal, the positions of the $4f^{n-1}5d$ levels are much more influenced by the crystal-field interaction than those of the $4f^n$ levels. The effect of crystal field on the 5d orbit will depress the level energies in a specific host lattices compared to the free ions. This is caused by a strong interaction of the 5d electron with the neighbouring anion ligands in the compound [17]. The lowest 4f5d state of Pr^{3+} in CAO has a slight red shift as compared with that in SAO, and also lies above the $^1S_0$ state. The onset absorptions of the Pr^{3+} 4f5d bands are at 212 nm (47 170 cm^{-1}) and 211 nm (47 393 cm^{-1}) in CAO and SAO, respectively, as shown in the inset. The lowest 4f5d level energy of Pr^{3+} in CAO is depressed more than that in SAO. In CAO:Pr^{3+} and SAO:Pr^{3+}, the Pr^{3+} ions replace Ca^{2+} and Sr^{2+}, respectively, and are in the same O^{2-} ion coordination environment (see figure 3). However, due to the relatively shorter cation–anion distance in CAO (average Ca–O distance ~2.71 Å) [18] than that in SAO (average Sr–O distance ~2.83 Å) [19], the crystal-field strength will be enhanced. And then, the energy of the lowest 4f5d state of Pr^{3+} in CAO will be depressed.

Besides these excitation bands, sharp lines peaking at 214 nm for both CAO:Pr^{3+} and SAO:Pr^{3+} are observed and can be assigned to the $^3H_4 \rightarrow {}^1S_0$ transition of Pr^{3+}. This line is very weak due to its strong forbidden character and in most cases it cannot be seen experimentally and it can only be estimated in the emission spectra or from theoretical calculation. From the position of the $^3H_4 \rightarrow {}^1S_0$ transition, the location of the $^1S_0$ state of Pr^{3+} in the two hosts can be determined both at 46 729 cm^{-1}. The energy difference between the $^1S_0$ state and the lowest 4f5d state is 441 cm^{-1} for CAO:Pr^{3+}, slightly smaller than that for SAO:Pr^{3+} (664 cm^{-1}).

It is well established that, ignoring any interaction between 5d and 4f electrons in the 4f5d configuration, the 5d electron of Pr^{3+} will experience the same crystal-field splitting and shift as that of Ce^{3+} in the same host [17, 32]. This means that the main splittings of the 4f5d configuration of Pr^{3+} and Ce^{3+} are the same. Moreover, there is a constant energy difference between the $4f \rightarrow 5d$ transition energy of Ce^{3+} and that of the $4f^2 \rightarrow 4f5d$ transitions of Pr^{3+}. This difference is independent of the type of host lattice. From the energetic positions of the lowest 5d level of Ce^{3+} (E_{Ce}), the energetic position of the lowest 4f5d level

of Pr^{3+} (E_{Pr}) in the same host can be estimated. In general, the following relation holds: $E_{Pr} = 12\,240 \pm 750$ cm^{-1} + E_{Ce}. By shifting the energy scale of the Ce^{3+} spectrum relative to the Pr scale using this relationship, the similarities between the two spectra can be revealed and the corresponding crystal-field components of the Pr^{3+} 4f5d states can be identified [17]. The relevant results for SAO:Pr^{3+} have been discussed by Dorenbos [32]. However, for CAO:Pr^{3+}, the crystal-field levels of the Pr^{3+} 4f5d states have not been demonstrated clearly. In figure 7 (curve 3), the five crystal-field levels of the Ce^{3+} 5d states in CAO have been shown by shifting the energy scale of the Ce^{3+} spectrum by 12 240 cm^{-1} relative to the Pr scale. The arrows indicate the possible locations of five unresolved 5d bands of Ce^{3+}. The resulting splitting pattern places the peaks in the excitation spectrum at 199 nm (50 251 cm^{-1}), 193 nm (51 813 cm^{-1}), 187 nm (53 475 cm^{-1}), 182 nm (54 545 cm^{-1}), and 175 nm (57 142 cm^{-1}). The anticipated splitting pattern is very consistent with the observed splitting of Pr^{3+}. The total crystal-field splitting is thus approximately 6891 cm^{-1}, which is slightly larger than that of Pr^{3+} in SAO ($\sim$6300 cm^{-1}). Following Dorenbos, irrespective of the type of anion coordination polyhedron around the Pr^{3+} ion, experimental data reveal an R^{-2} dependence of the magnitude of the splitting on the average distance R to the ligands. Then the larger splitting in CAO is also consistent with the relatively shorter R in CAO than that in SAO [33].

3.3. Effects of host excitation on Pr^{3+} luminescence

Upon VUV excitations of host lattice and different crystal-field levels of the Pr^{3+} 4f5d states, the emission spectra of CAO:1% Pr^{3+} are shown in figure 8. The characteristic emissions which display the QC process of Pr^{3+} at 402 nm (deep violet) and 485 nm (blue) are observed. Under excitation of the different crystal-field levels of the Pr^{3+} 4f5d states at 199, 193 and 187 nm, the relative intensities of blue to violet basically retain steady, while upon excitation of the host lattice at 170 and 140 nm, the blue emission will become more efficient than before, which means that the ET from the host to the $^1S_0$ and $^3P_0$ states is different. Especially, when the excitation wavelength (λ_{ex}) is smaller than 170 nm, the emission of the host lattice appears and the blue emission is more efficient than the violet. No changes of the branching ratio of the $^1S_0$ emissions can be found under different excitations. The excitation spectra of the violet and blue emissions are shown in the inset. Clearly, the host excitation around 170 nm for the blue emission is more efficient than those for the violet, which is consistent with the emission spectra above.

The situation found above was also encountered in SAO:Pr^{3+} [34]. To explain this, a mechanism of recombination and transfer of the energy from excitonic states to Pr^{3+} is proposed [8]. Across-band-gap excitation generates a number of free electrons in the conduction band (CB) and holes in the valence band (VB) of the crystal. The free holes will be converted to self-trapped holes (STHs) instantly, which can move at room temperature in the host. Some of them can reach activator centres and participate in their excitation processes. Others can capture free electrons from CB, creating self-trapped excitons (STEs). The STEs can decay radiatively or transfer their energies to the activators. However, after relaxation, most STEs have enough energy to populate the $^3P_0$ state, but not enough to feed the $^1S_0$ level. Thus, the luminescence from $^3P_0$ is excited more efficiently than $^1S_0$ under band-to-band excitation. The STE-mediated ET will result in the nonoccurrence of the QC process and reduce the possibilities of QC. For CAO:1% Pr^{3+}, the STEs can also undoubtedly be created with inter-band excitation, but the effects can almost be ignored because no obvious decrease of $^1S_0$ emission relative to $^3P_0$ can be found, e.g., under excitation of the lower 4f5d states ($\lambda_{ex} > 180$ nm), as shown in figure 8.

There exists STE-mediated ET not only in CAO:Pr^{3+} and SAO:Pr^{3+}, but in almost all Pr^{3+}-doped QC phosphors, including fluorides [35], aluminates [8], borates [8] and sulfates [36].
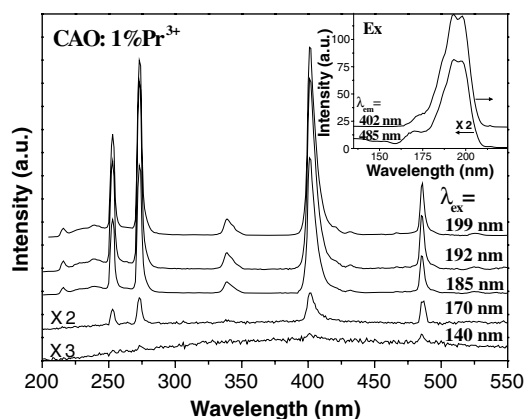
Figure 8. Emission spectra of CAO:1% Pr^{3+} upon excitations of host lattice (140 and 170 nm) and different crystal-field levels of Pr^{3+} 4f5d states (187, 193 and 199 nm). Inset: the excitation spectra of the 402 and 485 nm emissions of Pr^{3+}.

In the actual plasma display panel (PDP) and the mercury-free fluorescent lamp applications, the emitted radiation of the Xe dimer plasma lies in the VUV at 147 nm (8.4 eV, Xe monomer line) and around 172 nm (∼7.2 eV, Xe dimer band). As regards the currently applied VUV tricolour phosphors, the VUV light does not excite activators directly. The excitation energy is transferred from the host matrix to the luminescence centre. For this reason, current PDP phosphors must be phosphors with high-energy transfer from host lattice to activators. However, as regards the Pr^{3+}-doped QC phosphors, the host absorption induced STE-mediated ET will decrease the visible QE of QC. Consequently, host crystals with a fundamental absorption edge higher than the Xe discharge energy, at least not lower than Xe dimer band, are required to acquire practicable Pr^{3+}-doped QC phosphors. Fluorides are preferential in this case because they have the largest band gaps. However, fluoride phosphors are generally considered to be unstable and no lighting or display application makes use of a fluoride phosphor [37]. For aluminates, their host absorption bands overlap the Xe dimer band, as shown in figure 7. For borates and sulfates, their host absorption bands are both shorter than 160 nm [8]. However, they are not convenient materials for QC, because they offer high phonon vibrational frequencies, which result in the absence of emission from the $^3P_0$ state due to the efficient multi-phonon $^3P_0 \rightarrow {}^1D_2$ relaxation [6]. Therefore, by now, although more than a dozen of such Pr^{3+}-based QC phosphors have been identified, it would be useful to find more host lattices, which have a large forbidden gap (at least larger than 7.3 eV), have a low phonon frequency, and in which Pr^{3+} shows the QC phenomena.

3.4. Spectra overlap between Pr^{3+} and Cr^{3+}

As shown in figures 2 and 6, the Pr^{3+} emissions of $^1S_0 \rightarrow {}^1I_6$ at 402 nm and $^1S_0 \rightarrow {}^1G_4$ at 273 nm overlap Cr^{3+} excitations of $^4A_2 \rightarrow {}^4T_1(^4F)$ and $^4A_2 \rightarrow {}^4T_1(^4P)$, respectively. According to Forster–Dexter theory [9, 10], ET from Pr$^{3+1}S_0$ to Cr^{3+} is possible in the two hosts. However, it should be borne in mind that in a practical QC phosphor based on the Pr^{3+}–Cr^{3+} pair, the Pr^{3+} ion and not the Cr^{3+} ion should absorb the emission from the Xe discharge in the VUV region. As shown in figures 2 and 7, it becomes evident that Cr^{3+} ions will be involved in the absorption in addition to Pr^{3+} ions. Furthermore, for CAO:Pr^{3+}, Cr^{3+}, most of the absorptions of the Pr^{3+} 4f5d states are situated at wavelengths longer than

180 nm. Thus, the Xe discharge mostly excites the host absorption band and the CTB of Cr^{3+} instead of the intense Pr^{3+} 4f5d states. Therefore, in the VUV region the host absorption band and the Cr^{3+}-related CTB have an unfavourable overlap with the Pr^{3+} 4f5d states, preventing efficient selective Pr^{3+} excitation under radiation of Xe discharge, a prerequisite for the cascade emission of Pr^{3+}.

4. Conclusions

The optical spectroscopies between 150 and 750 nm of $CAO:M^{3+}$ (M = Pr, Cr) were investigated and compared with those of $SAO:M^{3+}$. R-line emissions are observed in $(C, S)AO:Cr^{3+}$. Cr^{3+} ions are found to replace the Al^{3+} ions and enter a strong crystal-field site in both hosts. In $CAO:Pr^{3+}$, relative to that in $SAO:Pr^{3+}$, the QE of Pr^{3+} $^3P_0$ is enhanced and the lowest 4f5d state of Pr^{3+} is depressed. There exist favourable spectral overlaps between Pr^{3+} $^1S_0$ emissions and the Cr^{3+} higher multiplets absorptions in CAO, which should promote the ET from $Pr^{3+1}S_0$ to Cr^{3+}. Upon across-band-gap excitation in the VUV region, the STE-mediated ET will result in preferential ET form host to low-lying Pr^{3+} $4f^2$ levels. In the actual applications, the Xe discharge mostly excites the host absorption bands and the CTB of Cr^{3+} instead of the intense Pr^{3+} 4f5d states in $(C, S)AO: Pr^{3+}, Cr^{3+}$, preventing efficient selective Pr^{3+} excitation, a prerequisite for the QC of Pr^{3+}.

Acknowledgments

References

[1] Ronda C 2002 *J. Lumin.* **100** 301
[2] Wegh R T, Donker H, Oskam K D and Meijerink A 1999 *Science* **283** 663
[3] Sommerdijk J L, Bril A and de Jager A W 1974 *J. Lumin.* **4** 288
[4] Piper W W, DeLuca J A and Ham F S 1974 *J. Lumin.* **8** 344
[5] Srivastava A M and Beers W W 1997 *J. Lumin.* **71** 285
[6] Srivastava A M, Doughty D A and Beers W W 1996 *J. Electrochem. Soc.* **143** 4113
[7] Srivastava A M, Doughty D A and Beers W W 1997 *J. Electrochem. Soc.* **144** 190
[8] van der Kolk E, Dorenbos P and van Eijk C W E 2001 *J. Phys.: Condens. Matter* **13** 5471
[9] Forster Th 1948 *Ann. Phys.* **2** 55
[10] Dexter D L 1953 *J. Chem. Phys.* **21** 836
[11] Zachau M, Zwaschka F and Kummer F 1997 *Electrochemical Society Conf. (Paris)*
[12] Zachau M, Zwaschka F and Kummer F 1998 *Proc. 6th Int. Conf. on Luminescent Materials* ed C R Ronda and T Welker (Princeton, NJ: Electrochemical Society) p 314
[13] van der Kolk E, Dorenbos P, van Eijk C W E, Vink A P, Weil M and Chaminade J P 2004 *J. Appl. Phys.* **95** 7867
[14] Wang X-J, Huang S, Lu L, Yen W M, Srivastava A M and Setlur A A 2001 *Opt. Commun.* **195** 405
[15] Chen Y, Shi C, Qi Z and Fu Y 2006 *Appl. Phys. Lett.* **88** 061906
[16] Fu Y, Zhang G, Qi Z, Wu W and Shi C 2006 *J. Lumin.* **124** 370
[17] Dorenbos P 2000 *J. Lumin.* **91** 91
[18] Utsunomiya A, Tanaka K, Morikawa H and Marumo F 1988 *J. Solid State Chem.* **75** 197
[19] Kimura K, Ohgaki M, Tanaka K, Morikawa H and Marumo F 1990 *J. Solid State Chem.* **87** 186
[20] Nie Z, Zhang J, Zhang X, Luo Y, Lu S and Wang X 2006 *J. Lumin.* **119/120** 332
[21] Nie Z, Zhang J, Wang X-J, Ren X and Zhang G 2006 *Electrochem. Soc. Trans.* at press
[22] Henderson B and Imbush G F 1989 *Optical Spectroscopy of Inorganic Solids* (Oxford: Oxford Science Publications)

[23] Sugano S J, Tanabe Y and Kamikura H 1970 *Multiplets of Transitions Metals Ions in Crystals* (New York: Academic)
[24] Tippins H H 1970 *Phys. Rev.* B **1** 126
[25] Blasse G and Grabmaier B 1995 *Luminescent Materials* (Berlin: Springer)
[26] Shannon R D 1976 *Acta Crystallogr.* A **32** 751
[27] Tanabe Y and Sugano S 1954 *J. Phys. Soc. Japan* **9** 753
[28] Nugent L J, Baybarz R D, Burnett J L and Ryan J L 1969 *J. Phys. Chem.* **73** 1177
[29] Orgel L E 1966 *An Introduction to Transition Metal Chemistry* (London: Methuen)
[30] Wamsley P R and Bray K L 1994 *J. Lumin.* **59** 11
[31] Huang S-H, Wang X-J, Chen B-J, Jia D and Yen W M 2003 *J. Lumin.* **102/103** 344
[32] Dorenbos P 2002 *J. Lumin.* **99** 283
[33] Dorenbos P 2002 *J. Alloys Compounds* **341** 156
[34] Rodnyi P A, Dorenbos P, Stryganyuk G B, Voloshinovskii A S, Potapov A S and van Eijk C W E 2003 *J. Phys.: Condens. Matter* **15** 719
[35] Vink A P, Dorenbos P, de Haas J T M, Donker H, Rodnyi P A, Avanesov A G and van Eijk C W E 2002 *J. Phys.: Condens. Matter* **14** 8889
[36] van der Kolk E, Dorenbos P, Vink A P, Perego R C, van Eijk C W E and Lakshmanan A R 2001 *Phys. Rev.* B **64** 195129
[37] Justel T, Nikol H and Ronda C 1998 *Angew. Chem. Int. Edn* **37** 3084